

Selective measurements of intertwined multipolar orders: Non-Kramers doublets on a triangular lattice

Changle Liu,¹ Yao-Dong Li,^{1,2} and Gang Chen^{1,3,4,*}

¹State Key Laboratory of Surface Physics and Department of Physics, Fudan University, Shanghai 200433, China

²Department of Physics, University of California Santa Barbara, Santa Barbara, California 93106, USA

³Center for Field Theory and Particle Physics, Fudan University, Shanghai, 200433, China

⁴Collaborative Innovation Center of Advanced Microstructures, Nanjing University, Nanjing 210093, China



(Received 10 May 2018; published 16 July 2018)

Motivated by the rapid experimental progress on the spin-orbit-coupled Mott insulators, we propose and study a generic spin model that describes the interaction between the non-Kramers doublets on a triangular lattice and is relevant for triangular lattice rare-earth magnets. We predict that the system supports both pure quadrupolar orders and intertwined multipolar orders in the phase diagram. Besides the multipolar orders, we explore the magnetic excitations to reveal the dynamic properties of the systems. Due to the peculiar properties of the non-Kramers doublets and the selective coupling to the magnetic field, we further study the magnetization process of the system in the magnetic field. We point out *the selective measurements* of the static and dynamic properties of the intertwined multipolarity in the neutron scattering, NMR, and μ SR probes and predict the experimental consequences. The relevance to the existing materials such as TmMgGaO_4 , Pr-based, and Tb-based magnets, and many ternary chalcogenides is discussed. Our results not only illustrate the rich physics and the promising direction in the interplay between strong spin-orbit-entangled multipole moments and the geometrical frustration, but also provide a general idea to use noncommutative observables to reveal the dynamics of the hidden orders.

DOI: [10.1103/PhysRevB.98.045119](https://doi.org/10.1103/PhysRevB.98.045119)

I. INTRODUCTION

There has been intensive activity and interest in correlated matters with strong spin-orbit coupling [1]. Various interesting quantum phases have been proposed, and the emergence of these rich phases is impossible in the absence of the strong spin-orbit coupling. More substantially, the abundance of candidate materials allows a rapid experimental progress of this field. In fact, the physical models for many relevant physical systems have not yet been constructed and thus not been explored carefully. This requires the knowledge of the microscopic nature of the relevant degrees of freedom. To establish the connection with the experimental observables, one needs to further understand the appearance of the physical properties for different phases of these newly constructed models. In this paper, we carry out these thoughts and study the spin-orbit-coupled Mott insulators with non-Kramers doublets on a triangular lattice.

Since the discovery and the proposal of the spin liquid candidate material YbMgGaO_4 [2–9], the triangular lattice rare-earth magnets have received more attention recently [4,10–24]. Many isostructural rare-earth magnets such as RCd_3P_3 , RZn_3P_3 , RCd_3As_3 , RZn_3As_3 [25–27], $\text{KBaR}(\text{BO}_3)_2$ [28] (R is a rare-earth atom), and many ternary chalcogenides [29,30] are now proposed. In these systems, the rare-earth atoms form a perfect triangular lattice. The combination of the spin-orbit coupling of the $4f$ electrons and the crystal electric field creates a local ground-state doublet that is described

by an effective spin-1/2 local moment at each rare-earth site. These rare-earth local moments then interact with each other and describe the low-temperature magnetic properties of the system. In most cases, the superexchange interaction is short-ranged, and nearest-neighbor exchange interaction with further neighbor dipolar interaction is sufficient due to the strong spatial localization of the $4f$ electron wave function. These materials provide a natural setting to study *the interplay between strong spin-orbit entanglement and geometrical frustration* in both theory and experiments.

In the list of relevant physical models for the rare-earth triangular lattice magnets, we have explored the usual Kramers doublets and the dipole-octupole doublets [31,32] in the previous works [4,10]. In particular, the anisotropic spin model [4,7] for the usual Kramers doublets was suggested to be

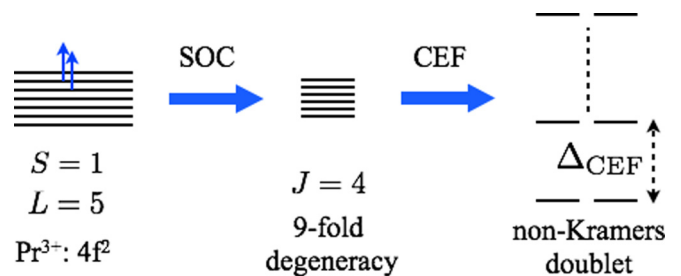


FIG. 1. The combination of spin-orbit coupling and the D_{3d} crystal electric field generates a non-Kramers doublet ground state for the Pr^{3+} ion. Here SOC refers to spin-orbit coupling, and CEF refers to crystal electric field. Other ions such as Tm^{3+} and Tb^{3+} could potentially support non-Kramers doublets.

*gangchen.physics@gmail.com

TABLE I. The relevant spin Hamiltonians for three different doublets on the triangular lattice. The models for the usual Kramers doublet and the dipole-octupole doublet have been obtained in the previous works.

Local doublets	The nearest-neighbor spin Hamiltonians on the triangular lattice	Reference
Usual Kramers doublet	$H = \sum_{(ij)} J_{zz} S_i^z S_j^z + J_{\pm} (S_i^+ S_j^- + S_i^- S_j^+) + J_{\pm\pm} (\gamma_{ij} S_i^+ S_j^+ + \gamma_{ij}^* S_i^- S_j^-) - \frac{iJ_{\pm\pm}}{2} [(\gamma_{ij}^* S_i^+ - \gamma_{ij} S_i^-) S_j^z + S_i^z (\gamma_{ij}^* S_j^+ - \gamma_{ij} S_j^-)]$	Refs. [3,4]
Dipole-octupole doublet	$H = \sum_{(ij)} J_z S_i^z S_j^z + J_x S_i^x S_j^x + J_y S_i^y S_j^y + J_{yz} (S_i^z S_j^y + S_i^y S_j^z)$	Ref. [10]
Non-Kramers doublet	$H = \sum_{(ij)} J_{zz} S_i^z S_j^z + J_{\pm} (S_i^+ S_j^- + S_i^- S_j^+) + J_{\pm\pm} (\gamma_{ij} S_i^+ S_j^+ + \gamma_{ij}^* S_i^- S_j^-)$	This paper

relevant for the spin liquid candidate YbMgGaO_4 and many other rare-earth triangular lattice magnets with Kramers ion. In this paper, we turn our attention to the non-Kramers doublet on the triangular lattice that has been advocated in the end of Ref. [4], and complete the full list of the microscopic spin models for the triangular lattice rare-earth magnets. Unlike the usual Kramers doublets, the mixed multipolar natures of spin components for the non-Kramers doublets greatly simplify the spin Hamiltonian. For the non-Kramers doublets [33–35], the longitudinal spin component behaves as the magnetic dipole moment, while the transverse spin components behave as the magnetic quadrupole moment. Therefore, the time-reversal symmetry and the hermiticity condition forbid the coupling between the longitudinal and the transverse components. Moreover, the ordering in the longitudinal spin components and the ordering in the transverse components have to be distinct and necessarily correspond to different phases and phase transitions. The purpose of this paper is to understand the intertwined multipolar ordering structures and the relevant experimental phenomena for the non-Kramers doublets on the triangular lattice.

The magnetic dipolar order can be directly visible through the conventional magnetic measurements such as the NMR and neutron diffraction experiments. The magnetic quadrupolar order (or, equivalently, spin nematicity) preserves the time-reversal symmetry and is often not quite visible in such conventional measurements. However, the dipole component that is orthogonal to the quadrupole component could then create quantum fluctuations for the quadrupole component and lead to coherent spin wave excitations. This *orthogonal effect* allows the detection of the spin wave spectra via the inelastic neutron scattering measurements. If the quadrupolar order breaks the translation symmetry and enlarges the unit cell, the symmetry-breaking pattern may not be quite visible in the static measurement, but is clear in the dynamic measurements. Thus, we study the magnetic excitations in the multipolar ordered phases. We establish the key connections between the underlying multipolar structure and the features in the excitation spectra. The orthogonal effect of the dipole component on the quadrupole component further lies in the coupling to the external magnetic field. The magnetic field only couples linearly to the dipole component and, thus, the magnetization and the magnetic susceptibility indirectly suggest the underlying quadrupolar order and transition.

The following part of the paper is organized as follows. In Sec. II, we propose the relevant physical model for the non-Kramers doublets on a triangular lattice and explain the physical significance of the spin operators. In Sec. III, we employ several different methods to obtain the full phase diagram of

this model. Since many states have an emergent $U(1)$ symmetry at the mean-field level, in Sec. IV, we study the quantum order by disorder phenomena for two representative states on our phase diagram. In Sec. V, we study the dynamic properties of the distinct phases that can serve as the experimental probes of the underlying multipolar orders. In Sec. VI, we point out the unique magnetization process due to the selective coupling of the moments to the external magnetic field. Finally, in Sec. VII, we discuss the experimental detection of various phases and summarize with a materials' survey. In Appendix A, we explain the relevance of the model to the Kitaev interaction. In Appendix B, we give the explanation of the non-Kramers doublet for the case of the spin-1 moments. In Appendix C, we show the complete spin wave dispersions for different phases.

II. MODEL HAMILTONIAN

Apart from YbMgGaO_4 , RCd_3P_3 , RZn_3P_3 , RCd_3As_3 , RZn_3As_3 , $\text{KBaR}(\text{BO}_3)_2$, and many ternary chalcogenides (LiRSe_2 , NaRS_2 , NaRSe_2 , KRS_2 , KRSe_2 , KRTe_2 , RbRS_2 , RbRSe_2 , RbRTe_2 , CsRS_2 , CsRSe_2 , CsRTe_2 , etc.) are known to have the rare-earth local moments on the triangular lattices, where R is the rare-earth atom. These chemical properties of the rare-earth atoms are quite similar, and thus it is often possible to substitute one for the other. A rare-earth ion, such as Yb^{3+} and Sm^{3+} , that contains odd number of electrons is the Kramers' ion and forms a ground-state doublet whose twofold degeneracy is protected by the time-reversal symmetry and the Kramers' theorem. A non-Kramers ion like Pr^{3+} and Tb^{3+} contains an even number of electrons per site (see Fig. 1). The spin-orbit coupling of the $4f$ electrons entangles the total spin moment and the orbital angular momentum, and leads to a total moment J that is an integer. The crystal electric field then splits the $2J + 1$ fold degeneracy and sometimes leads to a twofold degenerate ground-state doublet. Although both Kramers doublet and non-Kramers doublet are two-dimensional irreducible representations of the point group, the twofold degeneracy of the Kramers doublets is further protected by the time-reversal symmetry, and the degeneracy of the non-Kramers doublets is merely protected by the lattice symmetry. For these non-Kramers doublets, one then introduces an effective spin-1/2 operator, S_i , that acts on the twofold degenerate ground-state doublet at each lattice site (see Appendix B for a more detailed discussion for a specific case.)

Although the effective spin-1/2 operator is introduced to describe the non-Kramers doublet, the actual wave functions of the non-Kramers doublets are still integer spins in nature. As a result, the transformation of these effective spin-1/2 operators for the non-Kramers doublet is quite different from

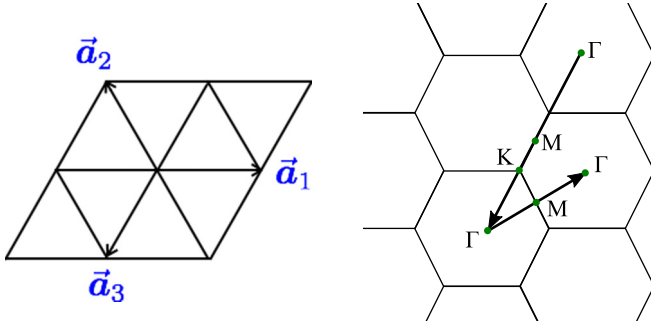


FIG. 2. (a) The triangular lattice with three distinct neighboring bonds and interactions. The phase parameter γ_{ij} depends on the bond orientation, which reflects the spin-orbit-entangled nature of the local moments. (b) The definition of the Brillouin zone for the triangular lattice.

the effective spin-1/2 operators for the Kramers doublet under the time-reversal symmetry. Specifically, the longitudinal component, S_i^z , is odd under time reversal and transforms as a magnetic dipole moment, and the transverse components, S_i^x and S_i^y , are even under time reversal and transform as the magnetic quadrupolar moment. Therefore, the generic symmetry-allowed spin Hamiltonian that describes the interaction between the non-Kramers doublets on the triangular lattice is simpler than the one for the Kramers doublets and is given as [4]

$$H = \sum_{\langle ij \rangle} J_{zz} S_i^z S_j^z + J_{\pm} (S_i^+ S_j^- + S_i^- S_j^+) + J_{\pm\pm} (\gamma_{ij} S_i^+ S_j^+ + \gamma_{ij}^* S_i^- S_j^-), \quad (1)$$

in which, γ_{ij} is a bond-dependent phase factor, and takes 1, $e^{i2\pi/3}$ and $e^{-i2\pi/3}$ on the $\mathbf{a}_1, \mathbf{a}_2$, and \mathbf{a}_3 bond (see Fig. 2), respectively. As shown in Table I, this model differs from the Kramers doublet model by the absence of the coupling between the transverse components and the longitudinal component.

Besides the standard expression of the model in Eq. (1), in Appendix A we further recast the model into a different form where the Kitaev interaction is explicitly shown.

III. PHASE DIAGRAM

In this section, we carry out several complementary approaches to determine the classical or mean-field phase diagram of the spin model defined in Eq. (1). The model is apparently frustrated, and a complicated phase diagram is expected.

We first notice that in the model, the spin rotation around the z direction by $\pi/4$ transforms $S^{\pm} \rightarrow \mp i S^{\pm}$ and the couplings in the model transform as

$$J_{zz} \rightarrow J_{zz}, \quad J_{\pm} \rightarrow J_{\pm}, \quad J_{\pm\pm} \rightarrow -J_{\pm\pm}. \quad (2)$$

Therefore, we can focus on the $J_{\pm\pm} > 0$ region of the phase diagram. Moreover, as most relevant materials are antiferromagnets, we choose $J_{zz} > 0$ in our analysis for the reason that will be clear later. Our results are summarized in Fig. 3 and Table II.

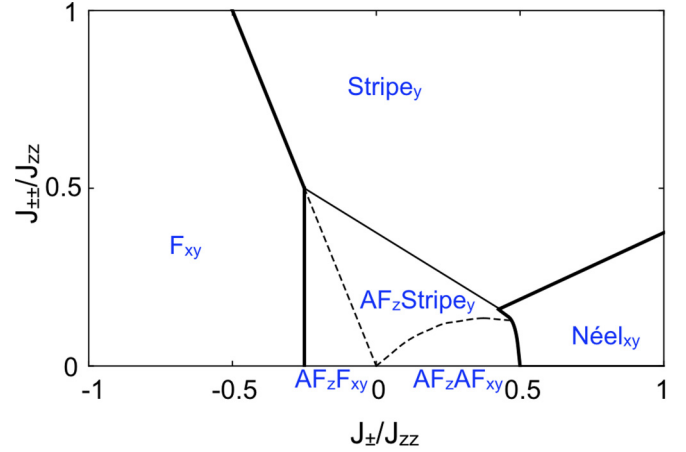


FIG. 3. The mean-field ground state phase diagram of the model in Eq. (1) with $J_{zz} > 0$. We find the Stripe_y state for large $J_{\pm\pm}$ regardless of the sign of J_{\pm} , the F_{xy} state for large negative J_{\pm} , and the Néel state for a large and positive J_{\pm} . Thick curves refer to first-order transitions, and thinner curves refer to second-order transitions. The dashed phase boundaries are determined by comparing the energy of AF_zStripe_y states with those of AF_z F_{xy} and AF_zAF_{xy}. The transitions across the dashed lines are complicated and may involve other competing states that are not well captured by our mean-field approach. The spin configurations of all ordered states are illustrated in Fig. 4.

A. Pure quadrupolar orders

To start with, we tackle this model in the spirit of a Weiss-type mean-field approach. This approach is qualitatively correct if the ground state of the spin model supports long-range orders with local on-site order parameters. This approach often provides some very basic information about the ground-state properties of the system. Within this approach, we treat the spin as a classical vector and optimize the energy by choosing a proper spin configuration. The classical spin vector is subjected to a local constraint $|S_i| = S$, and is thus often difficult to deal with. One can nevertheless try to solve for the ground state of the mean-field Hamiltonian with a relaxed global constraint, $\sum_i S_i^2 = NS^2$, where N is total number of spins, which does not necessarily respect the local spin constraint. When it does, this state is the actual classical ground state of the classical spin Hamiltonian. This method is often known as Luttinger-Tisza method [36].

In most parts of the phase diagram, the Luttinger-Tisza method can correctly reproduce the classical ground state. In the regimes where the method fails, we adopt a multisublattice mean-field ansatz to minimize the ground state energy. This approach is obviously simplified and cannot capture some of the more complicated magnetic orders or absence of magnetic orders due to strong frustration. The phase diagram obtained from mean-field theory is shown in Fig. 3. We found a family of long-range ordered phases as illustrated in Fig. 4. When one of the couplings is dominant, the frustration is suppressed, and the Luttinger-Tisza method works out well. This is the regime in which either J_{\pm} or $J_{\pm\pm}$ is dominant, and we have

TABLE II. The list of ordered phases in the phase diagram of Fig. 3.

States	Order types	Elastic neutron
F_{xy}	pure quadrupolar	no Bragg peak
120° Néel	pure quadrupolar	no Bragg peak
Stripe _y	pure quadrupolar	no Bragg peak
$AF_z F_{xy}$	intertwined multipolar	Bragg peak at K
$AF_z AF_{xy}$	intertwined multipolar	Bragg peak at K
AF_z Stripe _y	intertwined multipolar	Bragg peak at K

(1) F_{xy} state when J_{\pm} is large and negative. The ordering wave vector is at Γ point. In this state, the quadrupole components S^x and S^y align in the same direction in xy plane. At the mean-field level, this state has an emergent $U(1)$ degeneracy under the global rotation of an arbitrary angle about S^z . This is a bit surprising here since the microscopic model only has a discrete lattice symmetry due to the spin-orbit coupling. Thus, the emergent continuous degeneracy here and below is completely accidental, and quantum fluctuation beyond the mean-field theory should lift this degeneracy. This is the well-known order by quantum disorder. Moreover, due to this emergent continuous degeneracy, the excitation spectrum with respect to the quadrupolar order would have a pseudo-Goldstone mode that is nearly gapless. In Sec. IV, we carry out an explicit calculation to discuss this order by quantum disorder in this regime.

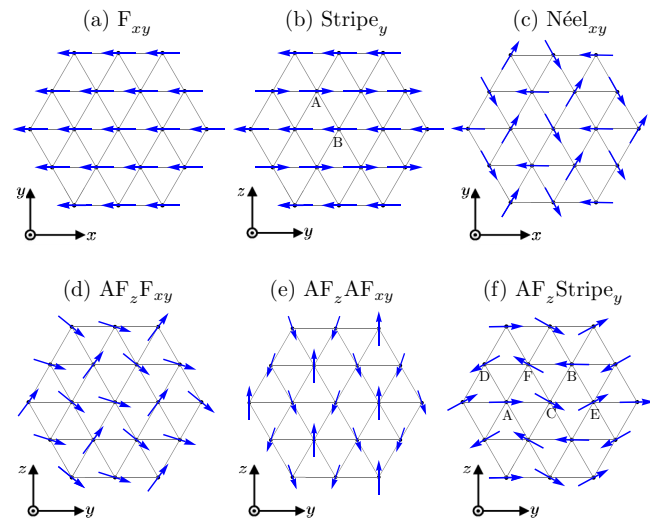


FIG. 4. Real-space spin configurations of the mean-field ground states found in Fig. 3. (a) The ferromagnetic quadrupolar order with spins aligned in xy plane, which we name the F_{xy} order. There is a global $U(1)$ degeneracy in the xy plane. (b) The antiferromagnetic quadrupolar stripe order with spins aligned in y direction, which we dub Stripe_y. (c), (d) The $AF_z F_{xy}$ and $AF_z AF_{xy}$ orders in Fig. 3 for small $J_{\pm\pm}$ and small J_{\pm} . Both orders have a three-sublattice structure, consistent with results from Refs. [37–39]. As in (b), the component in xy plane has a global $U(1)$ degeneracy for reasons explained in the text. (e) The 120° -Néel order stabilized by a large positive J_{\pm} . In all figures, we draw the coordinate system of the spin space to help visualization. The coordinate system of the real space always takes the same convention in Fig. 2.

(2) Stripe_y order when $J_{\pm\pm}$ is large. In this state, the quadrupolar component S^y is aligned in alternating directions for alternating rows of spins. The ordering wave vector is at M point. The spin-wave excitation is in general fully gapped.

(3) 120° Néel state with pure quadrupolar orders appears as the ground-state in the large J_{\pm} regime. In this state, spins lie in the xy plane and each spin is arranged 120° to its nearest neighbor, thus the ordering wave vector occurs at the K point. The state has nonvanishing quadrupolar components S^x and S^y . We find that this state has degenerate energies under effective spin rotation of arbitrary angle about S^z , so this state has emergent $U(1)$ degeneracy. For the same reason as the F_{xy} state, there would be a pseudo-Goldstone mode at Γ point.

The Néel and F_{xy} orders can be understood in the XXZ limit, where a large antiferromagnetic J_{\pm} induces the Néel order with the three-sublattice structure, and a large ferromagnetic J_{\pm} stabilizes the ferromagnetic order. The somewhat surprising emergent $U(1)$ symmetry is due to the canceling γ_{ij} phase factors of the anisotropic spin coupling term $J_{\pm\pm}$. The above three phases are purely quadrupolar orders, and are completely hidden in the magnetization measurements. Since they are absent of dipolar orders, even the elastic neutron scattering measurement cannot resolve these states. The dipolar spin component S^z , however, can create a coherent spin-wave excitation with respect to the quadrupolar ordered phases. Thus, despite the seemingly absence in the conventional magnetization measurements, the quadrupolar orders can nevertheless be detected via the inelastic neutron scattering experiments. We will explore this in Sec. IV.

B. Intertwined multipolar orders

Next we focus on the case with dominant J_{zz} that is presumably the most frustrated regime and thus supports strong quantum fluctuations. We here implement a traditional self-consistent Weiss mean-field theory by replacing the generic pair-wise spin interactions as

$$S_i^\mu S_j^\nu \rightarrow \langle S_i^\mu \rangle S_j^\nu + S_i^\mu \langle S_j^\nu \rangle - \langle S_i^\mu \rangle \langle S_j^\nu \rangle, \quad (3)$$

where $\langle S_i^\mu \rangle$ is the order parameter of the mean-field state and should be solved self-consistently. For this purpose, one first needs to set up a mean-field ansatz for the order parameters. From the experience of the XXZ model, one should at least choose a three-sublattice mean-field ansatz. Here, to be a bit more general, we choose a six-sublattice mean-field ansatz for some parameter regime. The local stability of the ground state is examined by the spin wave calculation. If the mean-field ground state is locally unstable, the spin wave spectra will no longer be real and positive.

Within this self-consistent mean-field approach, we find three types of intertwined multipolar long-range orders that are depicted in Figs. 3 and 4 and listed below,

(1) $AF_z F_{xy}$ for negative J_{\pm} and small $J_{\pm\pm}$. In this state, the spins have both nonzero antiferromagnetically ordered dipolar S^z and ferromagnetically ordered quadrupolar $S^{x,y}$ components. There is an emergent $U(1)$ degeneracy generated by the spin rotation about the S^z direction.

(2) $\text{AF}_z\text{AF}_{xy}$ for positive J_{\pm} and small $J_{\pm\pm}$. In this state, the spins have both nonzero antiferromagnetically ordered dipolar S^z and antiferromagnetically ordered quadrupolar $S^{x,y}$ components. This state also has the emergent $U(1)$ degeneracy in the xy plane of the spin space.

(3) $\text{AF}_z\text{Stripe}_y$ at larger $J_{\pm\pm}$. This phase is found proximate to Stripe_y phase via the second-order transition. It has a similar pattern with the Stripe_y state where the quadrupolar moment S^y orders in the stripelike pattern. It also develops magnetic order in the dipole component S^z .

All the above states carry intertwined multipolar orders, supporting both dipolar and quadrupolar orders. Here we provide the physical understanding for the emergence of these interesting orders. The AF_zF_{xy} and $\text{AF}_z\text{AF}_{xy}$ states are found to be the exact ground states in the XXZ limit where $J_{\pm\pm} = 0$, and are known as the supersolid orders in this limit, for which both the ‘‘boson density’’ S^z and the ‘‘superfluid order parameters’’ $S^{x,y}$ are nonvanishing. These supersolid orders are no longer the exact ground states for small values of $J_{\pm\pm}$. Moreover, the notion of ‘‘supersolidity’’ is ill-defined because the $J_{\pm\pm}$ interaction explicitly breaks the $U(1)$ spin rotational symmetry of the XXZ model. In fact, with a small $J_{\pm\pm}$ near the XXZ limit, the AF_zF_{xy} and $\text{AF}_z\text{AF}_{xy}$ states become unstable from our linear spin wave calculation and may turn into some incommensurate states. The incommensurate states are not well captured by our self-consistent mean-field approach that assumes commensurate states from the starting point. In the phase diagram, we nevertheless label the small $J_{\pm\pm}$ regime with the supersolid orders (AF_zF_{xy} and $\text{AF}_z\text{AF}_{xy}$ states).

The $\text{AF}_z\text{Stripe}_y$ state has intertwined dipolar S^z order and quadrupolar S^y order that result from the competition between $J_{\pm\pm}$ and J_{zz} . In the Ising limit with $J_{\pm\pm} \ll J_{zz}$, it is well-known that the ground-state manifold is extensively degenerate: the energy of a state is minimized as long as in each triangle Ising spins are not simultaneously parallel to each other. In the supersolid orders, this is manifested in the spin pattern where the signs of the S^z component is $(+, -, -)$ or $(+, +, -)$ in each triangle. Away from the Ising limit, a nonzero $J_{\pm\pm}$ allows the system to fluctuate within the extensively degenerate manifold of Ising spins, and therefore lifts the extensive degeneracy. This is quite analogous to the effect of the transverse field on top of the antiferromagnetic Ising interaction on the triangular lattice. The ground state in our case is such that the quadrupolar S^y component is maximized and ordered in a stripelike pattern to optimize the $J_{\pm\pm}$ term, while the dipolar S^z component orders in such a pattern where the signs of the S^z component is $(+, -, 0)$ in each triangle. As we show in Fig. 4, the combined structure of the dipolar and quadrupolar orders has a six-sublattice structure.

Unlike the pure quadrupolar order in the previous subsection, the intertwined multipolar orders are not completely invisible in the conventional magnetic measurement. The multiple-sublattice structure of the dipolar components can be detected through the usual bulk magnetization measurements such as NMR, μSR , and elastic neutron scattering measurements. Again, the quadrupolar orders hide themselves from such measurements. Thus, the intertwined multipolar nature is only partially visible.

Here, the presence of the intertwined multipolar order in this part of the phase diagram results from *the combination of*

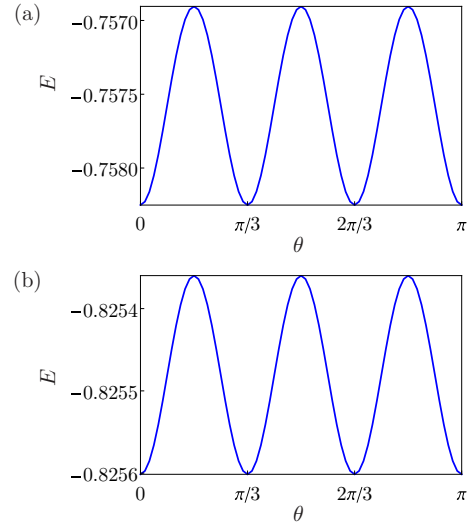


FIG. 5. Energy per spin taking into account quantum zero-point energy vs the azimuth angle θ of spins for (a) the F_{xy} state and (b) the 120° Néel $_{xy}$ state. Here we take the parameter $J_{\pm} = 0.4J_{zz}$, $J_{\pm\pm} = 0.4J_{zz}$ for the F_{xy} state and parameter $J_{\pm} = 0.9J_{zz}$, $J_{\pm\pm} = 0.2J_{zz}$ for the Néel $_{xy}$ state. The zero-point energy is calculated within the linear spin-wave method.

the geometrical frustration and the multipolar nature of the local moment. With only geometrical frustration, the system would simply support the conventional magnetic orders. With only spin-orbit-entangled local moments and the multipolar structure of the local moment, the system would not give an *intertwined* multipolar ordering structure. It is *the combination of the geometrical frustration and the multipolar nature of the local moment* that gives rise to the intertwined multipolar ordering structure.

IV. QUANTUM ORDER BY DISORDER

As we describe in previous sections, the system has only discrete spin-rotational symmetries, thus it is a bit counterintuitive that all phases except for Stripe_y phase in the mean-field phase diagram host emergent continuous $U(1)$ degeneracies in the xy plane of the spin space. These continuous degeneracies are due to nontrivial bond-dependent γ_{ij} phase factors in the $J_{\pm\pm}$ interactions. It should be noted that these continuous degeneracies are presented only at mean-field level, and in general should be lifted by quantum fluctuations. Here we study the quantum fluctuation in the F_{xy} state as an example. In the F_{xy} state, the mean-field state has spins align in xy plane with an arbitrary azimuth angle θ with respect to the x axis. If we take into account quantum fluctuations, these degenerate states will have different zero-point energies so that the degeneracy is lifted. This effect can be captured in the linear spin-wave theory. For $J_{\pm\pm} > 0$, it is shown in Fig. 5 that the quantum fluctuation selects the ground state with $\theta = n\pi/3$ ($n \in \mathbb{Z}$) such that the spins align along the bond orientations in the F_{xy} state. For the 120° Néel state, similar results are obtained, and the spins are aligned along the bond orientations. For other states with continuous degeneracies, we expect similar degeneracy breaking.

Here we present our linear spin-wave method that applies to multisublattice configurations [40–42]. Let us assume that the system has M -sublattice magnetic order. Each spin can be labeled by the magnetic unit cell index \mathbf{r} and sublattice index s . Assuming spins with sublattice index s has the direction pointing along the unit vector \mathbf{n}_s , one can always associate two unit vectors $\mathbf{u}_s \cdot \mathbf{n}_s = 0$ and $\mathbf{v}_s = \mathbf{n}_s \times \mathbf{u}_s$ so that \mathbf{n}_s , \mathbf{u}_s and \mathbf{v}_s are orthogonal with each other. Then we perform Holstein-Primakoff transformation for the spin operator $\mathbf{S}_{\mathbf{r}s}$,

$$\mathbf{n}_s \cdot \mathbf{S}_{\mathbf{r}s} = S - b_{\mathbf{r}s}^\dagger b_{\mathbf{r}s}, \quad (4)$$

$$(\mathbf{u}_s + i\mathbf{v}_s) \cdot \mathbf{S}_{\mathbf{r}s} = (2S - b_{\mathbf{r}s}^\dagger b_{\mathbf{r}s})^{\frac{1}{2}} b_{\mathbf{r}s}, \quad (5)$$

$$(\mathbf{u}_s - i\mathbf{v}_s) \cdot \mathbf{S}_{\mathbf{r}s} = b_{\mathbf{r}s}^\dagger (2S - b_{\mathbf{r}s}^\dagger b_{\mathbf{r}s})^{\frac{1}{2}}. \quad (6)$$

After performing Fourier transformation

$$b_{\mathbf{r}s} = \sqrt{\frac{M}{N}} \sum_{\mathbf{k} \in \overline{\text{BZ}}} b_{\mathbf{k}s} e^{i\mathbf{R}_s \cdot \mathbf{k}}, \quad (7)$$

the spin Hamiltonian can be rewritten in terms of boson bilinears as

$$H_{\text{sw}} = E_0 + \frac{1}{2} \sum_{\mathbf{k} \in \overline{\text{BZ}}} \left[\Psi(\mathbf{k})^\dagger h(\mathbf{k}) \Psi(\mathbf{k}) - \frac{1}{2} \text{tr} h(\mathbf{k}) \right], \quad (8)$$

where E_0 is the mean-field energy,

$$\Psi(\mathbf{k}) = [b_{\mathbf{k}1}, \dots, b_{\mathbf{k}M}, b_{-\mathbf{k}1}^\dagger, \dots, b_{-\mathbf{k}M}^\dagger]^T, \quad (9)$$

and $h(\mathbf{k})$ is a $2M \times 2M$ Hermitian matrix, and $\overline{\text{BZ}}$ is the magnetic Brillouin zone. H_{sw} can be diagonalized via a standard Bogoliubov transformation $\Psi(\mathbf{k}) = T_{\mathbf{k}} \Phi(\mathbf{k})$ where

$$\Phi(\mathbf{k}) = [\beta_{\mathbf{k}1}, \dots, \beta_{\mathbf{k}M}, \beta_{-\mathbf{k}1}^\dagger, \dots, \beta_{-\mathbf{k}M}^\dagger]^T, \quad (10)$$

and $T_{\mathbf{k}} \in SU(M, M)$. Here $SU(M, M)$ refers to indefinite special unitary group that is defined as [43]

$$SU(M, M) = \{g \in \mathbb{C}_{2M \times 2M} : g^\dagger \Sigma g = \Sigma, \det g = 1\}, \quad (11)$$

where Σ is the metric tensor and given as

$$\Sigma = \begin{pmatrix} I_{M \times M} & 0 \\ 0 & -I_{M \times M} \end{pmatrix}. \quad (12)$$

It is straightforward to prove that such transformation preserves the boson commutation rules. The diagonalized Hamiltonian reads

$$\begin{aligned} H_{\text{sw}} &= E_0 + \frac{1}{2} \sum_{\mathbf{k} \in \overline{\text{BZ}}} \left[\Phi(\mathbf{k})^\dagger E(\mathbf{k}) \Phi(\mathbf{k}) - \frac{1}{2} \text{tr} h(\mathbf{k}) \right] \\ &= E_0 + E_r + \sum_{\mathbf{k} \in \overline{\text{BZ}}} \omega_{\mathbf{k}s} \beta_{\mathbf{k}s}^\dagger \beta_{\mathbf{k}s}, \end{aligned} \quad (13)$$

where $E(\mathbf{k}) = \text{diag}[\omega_{\mathbf{k}1}, \dots, \omega_{\mathbf{k}M}, \omega_{-\mathbf{k}1}, \dots, \omega_{-\mathbf{k}M}]$ and

$$E_r = \frac{1}{4} \sum_{\mathbf{k} \in \overline{\text{BZ}}} \text{tr} [E(\mathbf{k}) - h(\mathbf{k})] \quad (14)$$

is the zero-point energy correction due to quantum fluctuations. Using this result, we obtain the quantum selection of the quadrupolar order in the F_{xy} state and the 120° Néel state.

Besides the quantum fluctuations, the continuous degeneracy could also be lifted by other interactions that are present in these systems. Due to the strong localization of the rare-earth electrons, further neighbor superexchange interactions can be quite small compared to nearest neighbors. However, the dipolar interaction between the S^z components can sometimes play some role. This Ising-like dipolar interaction may even modify the magnetic ground-state orders. We will examine the effect of the dipolar interaction on the anisotropic spin exchange interaction of the non-Kramers doublets in the future work.

V. DETECTION OF MULTIPOLAR ORDERS AND EXCITATIONS

As we have already indicated in the previous sections, the quadrupolar order is not directly visible from the conventional magnetic measurement. Instead, the dynamical measurement is able to observe the consequence of the quadrupolar orders. What is essential here is the noncommutative relation between the dipole component and the quadrupole component. It is this property that manifests the dynamics of the quadrupolar order in the S^z correlator. The dipole component, S^z , couples linearly with the external magnetic field. Likewise, the neutron spin would only couple to the dipole moment S^z at the linear order. Therefore, the inelastic neutron scattering would measure the S^z - S^z correlation,

$$\begin{aligned} S^{zz}(\mathbf{q}, \omega > 0) &= \frac{1}{2\pi N} \sum_{ij} \int_{-\infty}^{+\infty} dt e^{i\mathbf{q} \cdot (\mathbf{r}_i - \mathbf{r}_j) - i\omega t} \langle S_i^z(0) S_j^z(t) \rangle. \end{aligned} \quad (15)$$

In this section, we discuss the dynamic information of the system that is encoded in the inelastic neutron scattering measurements.

The remarkable feature of the *selective* coupling of the neutron spins to the magnetic moments greatly facilitates the identification of the intertwined multipolar orders. One can separately read off signatures of the ordering of dipole and quadrupole moments from elastic and inelastic neutron scattering measurements, respectively. The latter is because the S^z moment creates spin-flipping events on the quadrupole moments and thus creates coherent spin-wave excitations. These excitations then carry the information about the underlying quadrupolar ordering structures. Thus, although the quadrupolar moments do not directly couple to the magnetic field, the quadrupolar excitations can be indirectly probed. The dynamic spin structure factor, which is defined in Eq. (15) and measured by inelastic neutron scattering, encodes the dispersion and intensity of the quadrupolar excitations. In the following, we use the linear spin-wave theory to calculate the dynamic spin structure factor. We follow Ref. [42] and find that at zero temperature the dynamic spin structure factor takes

the form

$$S^{zz}(\mathbf{k}, \omega > 0) = \frac{S}{2M} \sum_{s=1}^M [T_{\mathbf{k}}^\dagger \mathbf{U}^z (\mathbf{U}^z)^\dagger T_{\mathbf{k}}]_{s+M, s+M} \delta(\omega - \omega_{\mathbf{k}s}), \quad (16)$$

where the $2M$ -dimensional vector \mathbf{U}^z is defined as

$$\mathbf{U}^z = [u_1^z + i v_1^z, u_2^z + i v_2^z, \dots, u_M^z + i v_M^z, u_1^z - i v_1^z, u_2^z - i v_2^z, \dots, u_M^z - i v_M^z]^T. \quad (17)$$

Here, we have neglected the two-magnon process in the above expression.

Our results are displayed in Fig. 6. The gapless modes in the figures are pseudo-Goldstone modes that arise from the emergent continuous degeneracy at the mean-field level and the linear spin-wave treatment. High-order quantum fluctuations would create a minigap for these modes. Despite that, we expect a T^2 heat capacity behavior for the temperature regime above the minigap energy scale in the ordered phase.

For our model that describes the spin-1/2 degrees of freedom, the number of magnon branches should be equal to the number of sublattices in the corresponding ordered phase. However, surprisingly, we find that for two-sublattice Stripe_y and six-sublattice AF_zStripe_y structures, we can see only one and three bands, respectively, which implies that half of the bands are completely invisible in the S^z - S^z correlator (see Appendix C for a comparison). The underlying reason is the

selection rule associated with the symmetry generated by

$$\hat{W} = T_{-\mathbf{a}_1 + \mathbf{a}_2} \otimes e^{i\pi \sum_j S_j^z}, \quad (18)$$

where $T_{-\mathbf{a}_1 + \mathbf{a}_2}$ denotes the lattice translation by $-\mathbf{a}_1 + \mathbf{a}_2$. The Hamiltonian stays invariant under \hat{W} , $[\hat{W}, H] = 0$.

From now on, we introduce the notation s and \bar{s} to denote the sublattice pair that is interchanged under the action of \hat{W} . In the labeling of Fig. 4, we find that $\bar{A} = B, \bar{C} = D, \bar{E} = F$.

For the elementary excitations, the effect of \hat{W} is such that

$$\text{Stripe}_y : \hat{W} b_{\mathbf{k},s} \hat{W}^\dagger = e^{i\phi(\mathbf{k})} b_{\mathbf{k},\bar{s}}, s = A, B, \quad (19)$$

$$\text{Stripe}_y \text{AF}_z : \hat{W} b_{\mathbf{k},s} \hat{W}^\dagger = e^{i\phi(\mathbf{k})} b_{\mathbf{k},\bar{s}}, s = A, \dots, F, \quad (20)$$

where $\phi(\mathbf{k}) = -k_x + k_y$.

The eigenmodes of \hat{W} take bonding/antibonding form,

$$\alpha_{\mathbf{k},s,\pm} = b_{\mathbf{k},s} \pm b_{\mathbf{k},\bar{s}}, \quad (21)$$

whose eigenvalues are

$$\hat{W} \alpha_{\mathbf{k},s,\pm} \hat{W}^\dagger = \pm e^{i\phi(\mathbf{k})} \alpha_{\mathbf{k},s,\pm}. \quad (22)$$

Since \hat{W} is a symmetry of the Hamiltonian, the energy eigenmodes are separate linear combinations of $\alpha_{\mathbf{k},s,\pm}$,

$$\beta_{\mathbf{k},t,\pm} = \sum_s c_{t,s} \alpha_{\mathbf{k},s,\pm} + d_{t,s} \alpha_{-\mathbf{k},s,\pm}^\dagger, \quad (23)$$

and

$$\hat{W} \beta_{\mathbf{k},t,\pm} \hat{W}^\dagger = \pm e^{i\phi(\mathbf{k})} \beta_{\mathbf{k},t,\pm}. \quad (24)$$

The \pm branches do not mix, since they have distinct eigenvalues under \hat{W} .

On the other hand, we can make a spectral representation of Eq. (15) as follows:

$$\begin{aligned} S^{zz}(\mathbf{q}, \omega > 0) &= \sum_n \langle 0 | \sum_{s=1}^M S_s^z(-\mathbf{q}, -\omega) | n \rangle \langle n | \sum_{s=1}^M S_s^z(\mathbf{q}, \omega) | 0 \rangle \\ &\propto \sum_n \delta(\omega - (\epsilon_n - \epsilon_0)) \langle 0 | \sum_{s=1}^M (b_{\mathbf{q},s} + b_{-\mathbf{q},s}^\dagger) | n \rangle \langle n | \sum_{s=1}^M (b_{-\mathbf{q},s} + b_{\mathbf{q},s}^\dagger) | 0 \rangle \\ &\propto \sum_n \delta(\omega - (\epsilon_n - \epsilon_0)) \langle 0 | \sum_{s=1}^M (\alpha_{\mathbf{q},s,+} + \alpha_{-\mathbf{q},s,+}^\dagger) | n \rangle \langle n | \sum_{s=1}^M (\alpha_{-\mathbf{q},s,+} + \alpha_{\mathbf{q},s,+}^\dagger) | 0 \rangle. \end{aligned} \quad (25)$$

It is thus obvious that the contribution is nonzero if and only if $|n\rangle$ is created by the $\beta_{\mathbf{k},t,+}$ operators. The $\beta_{\mathbf{k},t,-}$ states are not accessible. As a result, the S^z - S^z correlation function only measures coherent excitations with even parity. The odd parity excitations, instead, are present in S^x - S^x and S^y - S^y correlation functions.

The elastic neutron scattering measurement directly probes the magnetic ground state of the S^z components. The ordering wave vector of the dipolar moment S^z will be the magnetic Bragg peak in the static spin structure factor. For states with pure quadrupolar orders like F_{xy}, Stripe_y, and Néel_{xy}, there is no dipolar ordering and the ground state does not break time-reversal symmetry, so there are no Bragg peaks in static

spin structure factors. For states with intertwined multipolar orders such as AF_zF_{xy}, AF_zAF_{xy}, and AF_zStripe_y, however, the dipolar components order into a multisublattice pattern. The unit cell for the dipolar order is effectively enlarged, and hence one should observe the magnetic Bragg peaks at the K point in the Brillouin zone.

VI. THE MAGNETIZATION PROCESS

The peculiar property of the quadrupolar order and the non-Kramers doublets also lies in the magnetization process of the system under the external magnetic field. Although the magnetic field does not directly couple to the quadrupole

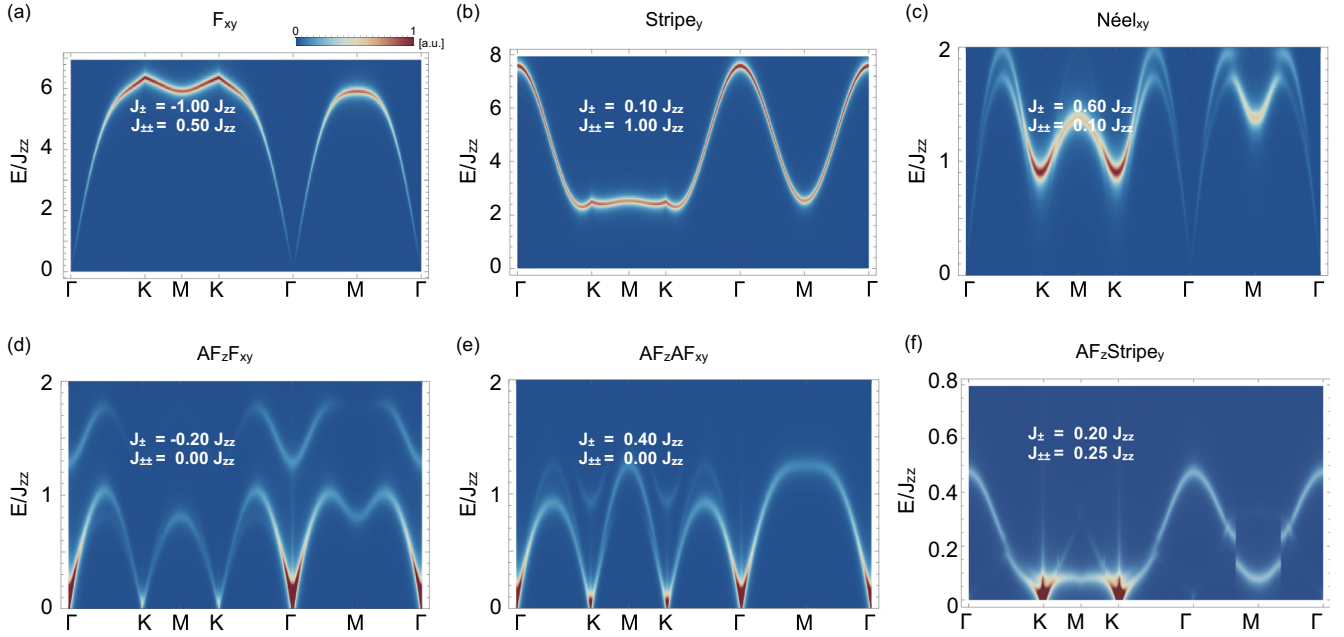


FIG. 6. Dynamic spin structure factors for the phases discussed in Sec. III, obtained from the linear spin-wave theory. The representative parameters for different subfigures are given. The plots here are intensity plots. We also plot the full spin-wave dispersions in Appendix C.

components of the local moment, the magnetization is influenced by the underlying quadrupolar order. The behavior of the magnetization should provide information about the hidden quadrupolar order that is otherwise not directly measurable. To explore this idea, we first introduce the magnetic field to the system so that we have

$$\begin{aligned} H_h &= H - g\mu_B h \sum_i S_i^z \\ &\equiv H - B \sum_i S_i^z. \end{aligned} \quad (26)$$

From the expression of the above Hamiltonian, one can immediately read off the Curie-Weiss temperature. Because the external magnetic field only couples to the S^z component of the local moment, the Curie-Weiss temperature only reflects the J_{zz} interaction, i.e.,

$$\Theta_{\text{CW}} = -\frac{3}{2}J_{zz}. \quad (27)$$

The impact of the underlying quadrupolar order on the magnetization should be most clear for the pure quadrupolar ordered phase. Here, we explore the physics on the Stripe_y state. The field will polarize the dipolar moments and suppress the quadrupolar ordering. In Fig. 7, we choose the coupling constants deep in the antiferroquadrupolar Stripe_y phase, where $J_{\perp} = 0.1J_{zz}$ and $J_{\pm\pm} = 1.0J_{zz}$. The mean-field ansatz is chosen to take care of the uniform S^z magnetization,

$$\langle S_i \rangle \equiv [m_i^x, m_i^y, m_i^z]^T = [0, e^{i\mathbf{M}\cdot\mathbf{R}_i} m^y, m^z]^T, \quad (28)$$

where $\mathbf{M} = (0, 2\pi/\sqrt{3})$ is the ordering wave vector for the Stripe_y state, and m^y, m^z real numbers subject to the constraint $|\langle S_i \rangle| = S$ for all sites i .

From the mean-field analysis, we plot the magnetization at zero and finite temperatures for different strengths of

transverse fields. In addition, the magnetic susceptibility and the dependence of the ordering temperature on the strength of the magnetic field are shown together in Fig. 7. We first discuss the zero field susceptibility χ^{zz} [see Fig. 7(a)]. Because of the lack of dipolar ordering, there is a constant χ^{zz} below T_c , and smoothly decays below T_c , obeying the Curie-Weiss law. In particular, it does not develop a peak across the finite-temperature transition at T_c , because the quadrupolar order parameter is “hidden” to the magnetic field. This is to be contrasted with the case of Kramers doublets, where the susceptibility shows a critical behavior at T_c .

The magnetic field suppresses the antiferroquadrupolar order. This is because the magnetization does not commute with the quadrupolar order parameter S^y . When the field polarizes the magnetization, the quantum fluctuation of the quadrupolar orders is enhanced and thereby reducing the ordering temperature. This physics has also been suggested for the electronic multipolar orders in intermetallic compounds TmAu_2 and TmAg_2 , where the lattice strain is introduced to control the electronic quadrupolar order [35]. Here we introduce the magnetic field to control the magnetization. In Figs. 7(b) and 7(c), we explicitly show this result from our mean-field theory.

Above the critical field B_c , the quadrupolar order is completely suppressed, and the dipolar moments are polarized by the field. The \mathbb{Z}_2 symmetry is generated by the rotation operation

$$\hat{U} \equiv e^{i\pi S^z}. \quad (29)$$

It is spontaneously broken in the antiferroquadrupolar ground states by $\langle S^y \rangle$ and is restored in the fully magnetized state. Around B_c , we expect a quantum critical region and quantum phase transition due to the breaking of the \mathbb{Z}_2 symmetry. Although the order parameter S^y cannot be directly measured, the

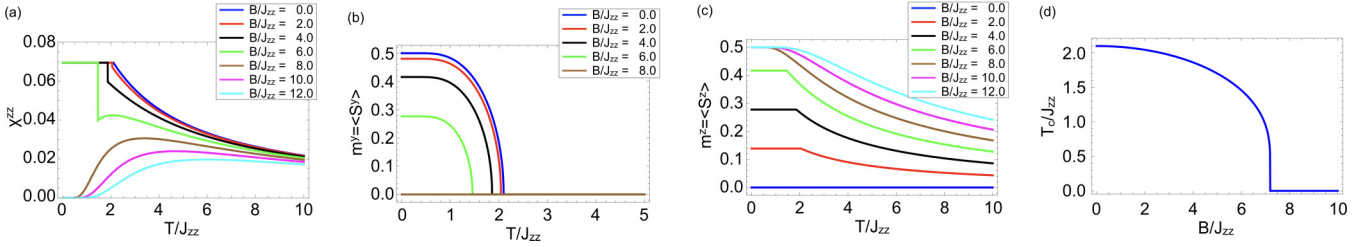


FIG. 7. (a) The magnetic susceptibility χ^{zz} at finite temperatures for different field strengths. There is a transition at $B_c \simeq 7.2J_{zz}$. (b) The antiferroquadrupolar order parameter at finite transversal fields and finite temperatures. (c) The dipolar moment at finite fields and finite temperatures. (d) The ordering temperature of the antiferroquadrupolar Stripe_y order as a function of transversal fields. In all figures we choose $J_{\pm} = 0.1J_{zz}$, and $J_{\pm\pm} = J_{zz}$, so that the ground state at zero field is in the Stripe_y phase.

quantum phase transition can be observed from the magnetic susceptibility at the finite B . In Fig. 7(d), we plot the transition temperature as a function of the external magnetic field.

The above analysis can be readily extended to F_{xy} , Néel, and other intertwined multipolar ordered phases. We have chosen the Stripe_y order as a representative. Going beyond the zero-temperature quantum limit, Ref. [44] has studied the interplay between distinct multipolar orders at finite temperatures in the presence of magnetic fields within a Ginzburg-Landau symmetry analysis. Our result here can be regarded as a quantum version of related physics.

VII. DISCUSSION

In this paper, we have established the phase diagram of the generic interacting model that is relevant for non-Kramers doublets on the triangular lattice. We find the broad existence of the pure quadrupolar orders and the intertwined multipolar orders in the phase diagram. Although the quadrupolar order is invisible from the conventional magnetic measurements, its presence shows up in the dynamic property and the magnetic excitations of the system. In contrast, the dipolar order can be directly measured by conventional magnetic probes. These unusual properties arise naturally from the selective coupling or measurement and the noncommutative relation between the dipolar and the quadrupolar moments. One could “read off” the dipolar order from the static magnetic probes and the quadrupolar order from the dynamic magnetic probes such as inelastic neutron scattering measurement.

In addition, we uncover the physics of the quantum order by disorder and the related pseudo-Goldstone modes. The consequences of this result appear both in the thermodynamics and the dynamic properties. Apart from the nearly gapless pseudo-Goldstone modes that show up in the dynamic measurements, the system in the relevant phases would have a T^2 heat capacity.

Here we point out the material’s relevance of our theoretical results. As we have mentioned in the beginning and in Sec. II, there exists an abundance of the triangular lattice rare-earth magnets. Most of these compounds have not been studied carefully, maybe not even been studied in any previous work. Among these materials, only the spin liquid candidate material YbMgGaO_4 has been studied extensively, both experimentally and theoretically. For others such as RCd_3P_3 , RZn_3P_3 ,

RCd_3As_3 , RZn_3As_3 , $\text{KBaR}(\text{BO}_3)_2$, and many ternary chalcogenides (LiRSe_2 , NaRS_2 , NaRSe_2 , KRS_2 , KRSe_2 , KRTe_2 , RbRS_2 , RbRSe_2 , RbRTe_2 , CsRS_2 , CsRSe_2 , CsRTe_2 , etc.) [25–30], little is known. When R^{3+} supports a non-Kramers doublet, our model and results can be directly applied. This could occur if R^{3+} ion is the Pr^{3+} , Tm^{3+} , or Tb^{3+} ion where the rare-earth ion contains an even number of $4f$ electrons per site. The single crystal TmMgGaO_4 was recently synthesized [45,46], and the lowest energy states of the Tm^{3+} ion were either a non-Kramers doublet or two nearly degenerate singlets [46]. In the latter case, the effective spin model should take into account of the effect from the crystal field splitting between two nearly degenerate singlets. Thus, the resulting model [47] would be fundamentally different from the model in Eq. (1). To resolve the single-ion ground state as well as the many-body ground state for TmMgGaO_4 , further crystal electric field study and experimental efforts are required.

Finally, our proposal for the selective measurement of the intertwined multipolar orders is not just specific to the non-Kramers doublets on triangular lattice. This piece of physics could be well extended to the non-Kramers doublets on other lattices. More broadly, any physical system with intertwined multipolar orders or hidden orders could potentially hold this kind of physics and phenomenon. The idea of *using noncommutative observables* to probe the dynamics of the hidden orders is central to our proposal and should be well extended to many other systems. These not only include the magnetic multipolar orders that are discussed in this paper but also contain the electronic analogues of the multipolar orders that have been discussed for example for the tetragonal intermetallic compounds TmAu_2 and TmAg_2 in Ref. [35] and for URu_2Si_2 [48].

ACKNOWLEDGMENTS

We acknowledge an ongoing collaboration with Professor Wenan Guo’s group from Beijing Normal University, and Professor Sasha Chernyshev from University of California Irvine for an email correspondence. This work is supported by the ministry of science and technology of China with the Grant No. 2016YFA0301001, the start-up fund and the first-class university construction fund of Fudan University, and the thousand-youth-talent program of China.

C.-L.L. and Y.-D.L. contributed equally to this paper.

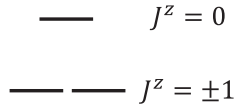


FIG. 8. The non-Kramers ground state doublet from splitting the spin-1 triplets.

APPENDIX A: THE RELEVANCE OF OUR MODEL TO KITAEV INTERACTION

In a previous work [49], we have pointed out that the vast numbers of rare-earth magnets can support the Kitaev interaction. This means the Kitaev interaction goes much beyond the iridate system that was previously proposed [50], and we illustrated the observation from the rare-earth double perovskites [49]. A similar suggestion was made for Co-based magnets [51,52]. Here we extend our idea to our model on the triangular lattice.

Generally speaking, a system with a local on-site threefold rotational symmetry and spin-orbit-entangled doublets (except dipole-octupole doublets) would necessarily have a Kitaev interaction. These lattices include honeycomb lattice, triangular lattice, pyrochlore lattice, FCC lattice, etc. Our results can be well extended to these lattices. The threefold rotation permutes the bonds connecting to the lattice site of the rotational center, and at the same time, permutes the spin components. For our triangular lattice, we define

$$S_i^a \equiv \sqrt{\frac{2}{3}} S_i^x + \sqrt{\frac{1}{3}} S_i^z, \quad (\text{A1})$$

$$S_i^b \equiv \sqrt{\frac{2}{3}} \left(-\frac{1}{2} S_i^x + \frac{\sqrt{3}}{2} S_i^y \right) + \sqrt{\frac{1}{3}} S_i^z, \quad (\text{A2})$$

$$S_i^c \equiv \sqrt{\frac{2}{3}} \left(-\frac{1}{2} S_i^x - \frac{\sqrt{3}}{2} S_i^y \right) + \sqrt{\frac{1}{3}} S_i^z, \quad (\text{A3})$$

then our Hamiltonian in Eq. (1) is recast into the following form:

$$\begin{aligned}
 H = & \sum_{(ij) \in \alpha} \left[J S_i \cdot S_j + K S_i^\alpha S_j^\alpha \right. \\
 & + \sum_{\beta, \gamma \neq \alpha} \Gamma (S_i^\alpha S_j^\beta + S_i^\beta S_j^\alpha + S_i^\alpha S_j^\gamma + S_i^\gamma S_j^\alpha) \\
 & \left. + \sum_{\beta, \gamma \neq \alpha} (K + \Gamma) (S_i^\beta S_j^\gamma + S_i^\gamma S_j^\beta) \right], \quad (\text{A4})
 \end{aligned}$$

where $\alpha = a, b, c$ labels the nearest-neighbor bond, the a bond corresponds to the \mathbf{a}_1 bond, the b bond corresponds to the \mathbf{a}_2 bond, and the c bond corresponds to the \mathbf{a}_3 bond. The couplings in the above equation are related to the ones in the main context as follows:

$$J = \frac{4}{3} J_\pm - \frac{2}{3} J_{\pm\pm} + \frac{1}{3} J_{zz}, \quad (\text{A5})$$

$$K = 2J_{\pm\pm}, \quad (\text{A6})$$

$$\Gamma = -\frac{2}{3} J_\pm - \frac{2}{3} J_{\pm\pm} + \frac{1}{3} J_{zz}. \quad (\text{A7})$$

APPENDIX B: DEFINITION OF EFFECTIVE SPIN-1/2 OPERATORS FOR THE NON-KRAMERS DOUBLET

To give a simple illustration about the property of the non-Kramers doublet, we discuss the case for the spin-1 local moment \mathbf{J} . Assuming a single-ion anisotropy $-D_z(J^z)^2$ (with $D_z > 0$), the three spin states are split into two lower doublets $J^z = \pm 1$ and an upper singlet $J^z = 0$. The energy levels are shown in Fig. 8. The $J^z = \pm 1$ states can be thought of as a non-Kramers doublet. We thus define the effective spin-1/2 operators \mathbf{S} from the physical spin operators \mathbf{J} ,

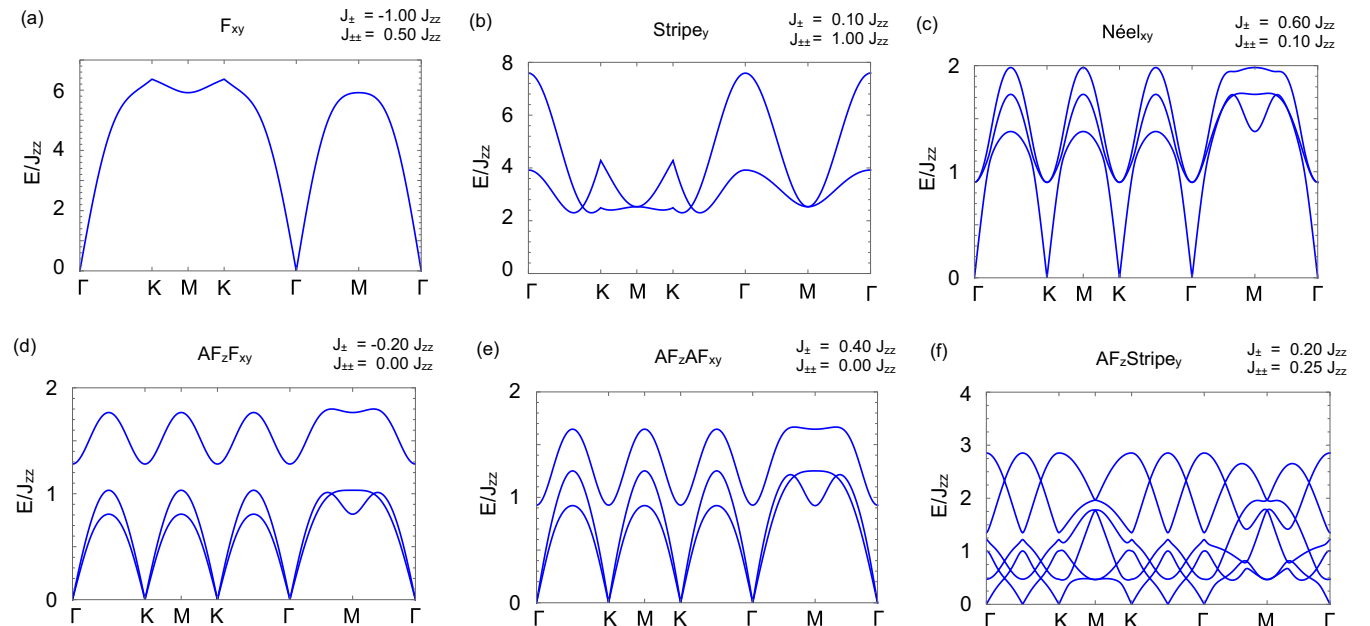


FIG. 9. The complete spin-wave dispersions for different phases. The parameters are chosen to be the same as in Fig. 6. The plots of the full dispersions here are to be compared with the intensity plots in Fig. 6.

such that

$$S^z = \frac{1}{2} P J^z P, \quad (\text{B1})$$

$$S^\pm = \frac{1}{2} P (J^\pm)^2 P, \quad (\text{B2})$$

where $S^\pm = S^x \pm i S^y$, $J^\pm = J^x \pm i J^y$, and P is the projection operator onto the $J^z = \pm 1$ subspace. The effective spin operators defined above satisfy the canonical commutation relation,

$$[S^a, S^b] = i \epsilon_{abc} S^c. \quad (\text{B3})$$

We further identify S^z as the dipolar moment and $S^{x,y}$ as the quadrupolar moment by examining their transformation under

time-reversal operation,

$$\Theta^{-1} S^z \Theta = -S^z, \quad (\text{B4})$$

$$\Theta^{-1} S^x \Theta = S^x, \quad (\text{B5})$$

$$\Theta^{-1} S^y \Theta = S^y. \quad (\text{B6})$$

APPENDIX C: SPIN-WAVE DISPERSION

In this Appendix, we plot the dispersion of all spin-wave branches. Compared with Fig. 6, we see in Fig. 9 that only some of the bands are visible in neutron scattering experiments.

-
- [1] W. Witczak-Krempa, G. Chen, Y. B. Kim, and L. Balents, Correlated quantum phenomena in the strong spin-orbit regime, *Annu. Rev. Condens. Matter Phys.* **5**, 57 (2014).
- [2] Y. Li, H. Liao, Z. Zhang, S. Li, F. Jin, L. Ling, L. Zhang, Y. Zou, L. Pi, Z. Yang, J. Wang, Z. Wu, and Q. Zhang, Gapless quantum spin liquid ground state in the two-dimensional spin-1/2 triangular antiferromagnet YbMgGaO₄, *Sci. Rep.* **5**, 16419 (2015).
- [3] Y. Li, G. Chen, W. Tong, L. Pi, J. Liu, Z. Yang, X. Wang, and Q. Zhang, Rare-Earth Triangular Lattice Spinliquid: A Single-Crystal Study of YbMgGaO₄, *Phys. Rev. Lett.* **115**, 167203 (2015).
- [4] Y.-D. Li, X. Wang, and G. Chen, Anisotropic spin model of strong spin-orbit-coupled triangular antiferromagnets, *Phys. Rev. B* **94**, 035107 (2016).
- [5] Y. Shen, Y.-D. Li, H. Wo, Y. Li, S. Shen, B. Pan, Q. Wang, H. C. Walker, P. Steffens, M. Boehm, Y. Hao, D. L. Quintero-Castro, L. W. Harriger, L. Hao, S. Meng, Q. Zhang, G. Chen, and J. Zhao, Spinon Fermi surface in a triangular lattice quantum spin liquid YbMgGaO₄, *Nature* **540**, 559 (2016).
- [6] J. A. M. Paddison, Z. Dun, G. Ehlers, Y. Liu, M. B. Stone, H. Zhou, and M. Mourgil, Continuous excitations of the triangular-lattice quantum spin liquid YbMgGaO₄, *Nat. Phys.* **13**, 117 (2017).
- [7] Y.-D. Li, Y. Shen, Y. Li, J. Zhao, and G. Chen, Effect of spin-orbit coupling on the effective-spin correlation in YbMgGaO₄, *Phys. Rev. B* **97**, 125105 (2018).
- [8] Y.-D. Li, Y.-M. Lu, and G. Chen, Spinon Fermi surface U(1) spin liquid in the spin-orbit-coupled triangular-lattice Mott insulator YbMgGaO₄, *Phys. Rev. B* **96**, 054445 (2017).
- [9] Y. Li, D. Adroja, P. K. Biswas, P. J. Baker, Q. Zhang, J. Liu, A. A. Tsirlin, P. Gegenwart, and Q. Zhang, Muon Spin Relaxation Evidence for the U(1) Quantum Spin-Liquid Ground State in the Triangular Antiferromagnet YbMgGaO₄, *Phys. Rev. Lett.* **117**, 097201 (2016).
- [10] Y.-D. Li, X. Wang, and G. Chen, Hidden multipolar orders of dipole-octupole doublets on a triangular lattice, *Phys. Rev. B* **94**, 201114 (2016).
- [11] C. Liu, R. Yu, and X. Wang, Semiclassical ground-state phase diagram and multi- q phase of a spin-orbit-coupled model on triangular lattice, *Phys. Rev. B* **94**, 174424 (2016).
- [12] Q. Luo, S. Hu, B. Xi, J. Zhao, and X. Wang, Ground-state phase diagram of an anisotropic spin- $\frac{1}{2}$ model on the triangular lattice, *Phys. Rev. B* **95**, 165110 (2017).
- [13] Z. Ma, J. Wang, Z.-Y. Dong, J. Zhang, S. Li, S.-H. Zheng, Y. Yu, W. Wang, L. Che, K. Ran, S. Bao, Z. Cai, P. Čermák, A. Schneidewind, S. Yano, J. S. Gardner, X. Lu, S.-L. Yu, J.-M. Liu, S. Li, J.-X. Li, and J. Wen, Spin-Glass Ground State in a Triangular-Lattice Compound YbZnGaO₄, *Phys. Rev. Lett.* **120**, 087201 (2018).
- [14] E. Parker and L. Balents, Finite-temperature behavior of a classical spin-orbit-coupled model for YbMgGaO₄ with and without bond disorder, *Phys. Rev. B* **97**, 184413 (2018).
- [15] Y. Xu, J. Zhang, Y. S. Li, Y. J. Yu, X. C. Hong, Q. M. Zhang, and S. Y. Li, Absence of Magnetic Thermal Conductivity in the Quantum Spin-Liquid Candidate YbMgGaO₄, *Phys. Rev. Lett.* **117**, 267202 (2016).
- [16] S. Toth, K. Rolfs, A. R. Wildes, and C. Ruegg, Strong exchange anisotropy in YbMgGaO₄ from polarized neutron diffraction, *arXiv:1705.05699*.
- [17] L. Yuesheng, D. Adroja, D. Voneshen, R. I. Bewley, Q. Zhang, A. A. Tsirlin, and P. Gegenwart, Nearest-neighbor resonating valence bonds in YbMgGaO₄, *Nat. Commun.* **8**, 15814 (2017).
- [18] Y. Li, D. Adroja, R. I. Bewley, D. Voneshen, A. A. Tsirlin, P. Gegenwart, and Q. Zhang, Crystalline Electric-Field Randomness in the Triangular Lattice Spin-Liquid YbMgGaO₄, *Phys. Rev. Lett.* **118**, 107202 (2017).
- [19] Y. Shen, Y.-D. Li, H. C. Walker, P. Steffens, M. Boehm, X. Zhang, S. Shen, H. Wo, G. Chen, and J. Zhao, Fractionalized excitations in the partially magnetized spin liquid candidate YbMgGaO₄, *arXiv:1708.06655*.
- [20] J. Iaconis, C. Liu, G. B. Halász, and L. Balents, Spin liquid versus spin orbit coupling on the triangular lattice, *SciPost Phys.* **4**, 003 (2018).
- [21] Z. Zhu, P. A. Maksimov, S. R. White, and A. L. Chernyshev, Disorder-Induced Mimicry of a Spin Liquid in YbMgGaO₄, *Phys. Rev. Lett.* **119**, 157201 (2017).
- [22] Z.-X. Luo, E. Lake, J.-W. Mei, and O. A. Starykh, Spinon Magnetic Resonance of Quantum Spin Liquids, *Phys. Rev. Lett.* **120**, 037204 (2018).

- [23] I. Kimchi, A. Nahum, and T. Senthil, Valence Bonds in Random Quantum Magnets: Theory and Application to YbMgGaO_4 , [arXiv:1710.06860](#).
- [24] Z. Zhu, P. A. Maksimov, S. R. White, and A. L. Chernyshev, Topography of Spin Liquids on a Triangular Lattice, *Phys. Rev. Lett.* **120**, 207203 (2018).
- [25] S. S. Stoyko and A. Mar, Ternary rare-earth zinc arsenides $\text{REZn}_{1-x}\text{As}_2$ (RE=La-Nd, Sm), *J. Solid State Chem. France* **184**, 2360 (2011).
- [26] A. T. Nientiedt and W. Jeitschko, The series of rare earth zinc phosphides RZn_3P_3 (R=Y, La-Nd, Sm, Gd-Er) and the corresponding cadmium compound PrCd_3P_3 , *J. Solid State Chemistry France* **146**, 478 (1999).
- [27] A. Yamada, N. Hara, K. Matsubayashi, K. Munakata, C. Ganguli, A. Ochiai, T. Matsumoto, and Y. Uwatoko, Effect of pressure on the electrical resistivity of CeZn_3P_3 , *J. Phys. Conf. Ser.*, **215**, 012031 (2010).
- [28] V. S. Shevchenko, N. G. Kononova, A. E. Kokh, A. K. Bolatov, B. M. Uralbekov, and M. M. Burkitbaev, $\text{KBaR}(\text{BO}_3)_2$ orthoborates (R = RE): Synthesis and study, *Russ. J. Inorg. Chem.* **62**, 1177 (2017).
- [29] T. Ohtani, H. Honjo, and H. Wada, Synthesis, Order-disorder transition and magnetic properties of LiLnS_2 , LiLnSe_2 , NaLnS_2 and NaLnSe_2 (Lnlanthanides), *Mater. Res. Bull.* **22**, 829 (1987).
- [30] M. Sato, G. Adachi, and J. Shiokawa, Preparation and structure of sodium rare-earth sulfides, NaLnS_2 (Ln; Rare earth elements), *Mater. Res. Bull.* **19**, 1215 (1984).
- [31] Y.-P. Huang, G. Chen, and M. Hermele, Quantum Spin Ices and Topological Phases from Dipolar-Octupolar Doublets on the Pyrochlore Lattice, *Phys. Rev. Lett.* **112**, 167203 (2014).
- [32] Y.-D. Li and G. Chen, Symmetry enriched U(1) topological orders for dipole-octupole doublets on a pyrochlore lattice, *Phys. Rev. B* **95**, 041106 (2017).
- [33] S. Lee, S. Onoda, and L. Balents, Generic quantum spin ice, *Phys. Rev. B* **86**, 104412 (2012).
- [34] S. Onoda and Y. Tanaka, Quantum Melting of Spin Ice: Emergent Cooperative Quadrupole and Chirality, *Phys. Rev. Lett.* **105**, 047201 (2010).
- [35] A. V. Maharaj, E. W. Rosenberg, A. T. Hristov, E. Berg, R. M. Fernandes, I. R. Fisher, and S. A. Kivelson, Transverse fields to tune an Ising-nematic quantum critical transition, [arXiv:1704.07841](#).
- [36] J. M. Luttinger and L. Tisza, Theory of dipole interaction in crystals, *Phys. Rev.* **70**, 954 (1946).
- [37] S. Wessel and M. Troyer, Supersolid Hard-Core Bosons on the Triangular Lattice, *Phys. Rev. Lett.* **95**, 127205 (2005).
- [38] R. G. Melko, A. Paramakanti, A. A. Burkov, A. Vishwanath, D. N. Sheng, and L. Balents, Supersolid Order from Disorder: Hard-Core Bosons on the Triangular Lattice, *Phys. Rev. Lett.* **95**, 127207 (2005).
- [39] D. Yamamoto, G. Marmorini, and I. Danshita, Quantum Phase Diagram of the Triangular-Lattice XXZ Model in a Magnetic Field, *Phys. Rev. Lett.* **112**, 127203 (2014).
- [40] S. Petit, Numerical simulations and magnetism, *JDN* **12**, 105 (2011).
- [41] D. C. Wallace, Spin waves in complex lattices, *Phys. Rev.* **128**, 1614 (1962).
- [42] S. Toth and B. Lake, Linear spin wave theory for single-Q incommensurate magnetic structures, *J. Phys.: Condens. Matter* **27**, 166002 (2015).
- [43] R. Goodman and N. R. Wallach, *Symmetry, Representations, and Invariants*, Vol. 66 (Springer, Berlin, 2009).
- [44] S. Lee, S. Trebst, Y. B. Kim, and A. Paramakanti, Landau theory of multipolar orders in $\text{Pr}(\text{TM})_2\text{X}_{20}$ Kondo materials, [arXiv:1806.02842](#).
- [45] F. A. Cevallos, K. Stolze, T. Kong, and R. J. Cava, Anisotropic magnetic properties of the triangular plane lattice material TmMgGaO_4 , [arXiv:1710.07707](#) [cond-mat.mtrl-sci].
- [46] Y. Li, S. Bachus, Y. Tokiwa, A. A. Tsirlin, and P. Gegenwart, Absence of zero-point entropy in a triangular Ising antiferromagnet, [arXiv:1804.00696](#).
- [47] C. Liu and G. Chen (unpublished).
- [48] J. A. Mydosh and P. M. Oppeneer, Colloquium: Hidden order, superconductivity, and magnetism: The unsolved case of URu_2Si_2 , *Rev. Mod. Phys.* **83**, 1301 (2011).
- [49] F.-Y. Li, Y.-D. Li, Y. Yu, A. Paramakanti, and G. Chen, Kitaev materials beyond iridates: Order by quantum disorder and Weyl magnons in rare-earth double perovskites, *Phys. Rev. B* **95**, 085132 (2017).
- [50] G. Jackeli and G. Khaliullin, Mott Insulators in the Strong Spin-Orbit Coupling Limit: From Heisenberg to a Quantum Compass and Kitaev Models, *Phys. Rev. Lett.* **102**, 017205 (2009).
- [51] H. Liu and G. Khaliullin, Pseudospin exchange interactions in d^7 cobalt compounds: Possible realization of the Kitaev model, *Phys. Rev. B* **97**, 014407 (2018).
- [52] R. Sano, Y. Kato, and Y. Motome, Kitaev-Heisenberg Hamiltonian for high-spin d^7 Mott insulators, *Phys. Rev. B* **97**, 014408 (2018).